PAPER • **OPEN ACCESS**

Compressor fouling detection by image analysis

To cite this article: A Suman *et al* 2023 *J. Phys.: Conf. Ser.* **2511** 012001

Compressor fouling detection by image analysis

A Suman, N Zanini, M Pinelli

Department of Engineering – DE, University of Ferrara, 44122 Ferrara, Italy

Corresponding author: Alessio Suman - alessio.suman@unife.it

Abstract. Gas turbine fouling is commonly known as responsible for performance degradation in terms of compression ratio and efficiency. The adhesion of micro-sized particles (soil, soot, salt, etc.) caused the modification of the blade shapes and the surface roughness. Both of these two effects determine the modification of the compressor performance over the unit operation. Due to the lack of capability to forecast the fouling intensity, it could be useful to estimate the fouling intensity during the machine overhaul, collecting strategical data by which a specific characterization of a given machine in a given operating site can be done. The present paper proposes and validates a helpful methodology for estimating the deposit intensity by an image analysis procedure. An image-detection technique has been carried out before and after the contamination process, and, using a subtraction process, a quantitative analysis of the fouled regions can be developed. The results show that, with a careful light and camera setup, the intensity of the deposits can be estimated with an acceptable tolerance band, which allows the possibility of collecting quantitative data on compressor deposits during overhaul operations. This generates a valuable starting point for predicting the overtime degradation of the unit and/or estimating the filtration section efficiency.

1. Introduction

Several energy consumptions and emission constraints focus on every energy transformation and consumption. Therefore, the straightforward way to reduce energy consumption is to increase the efficiency of the devices and systems. In light of this new technology era, gas turbines represent such systems able to easily convert energy in a very small footprint area, making these engines useful for the energy transition process [1, 2].

The gas turbine technology has been developed to increase its efficiency using new technology and design by incrementing the firing temperature and aerodynamic performance and decreasing emissions and fuel consumption. However, gas turbines experience performance degradation during operation due to flow path contamination [3, 4]. This effect is generated by the adhesion of micro-sized particles from fuel and/or the environment [5, 6]. The contamination provided by the fuel impurity affects the turbine section (hot section of the gas turbine, after the combustor), and it can be slowed down by adopting cleaner fuel. By contrast, the contamination provided by the airborne contaminant can be slowed down by inlet filtering sections, but in several applications, the filtration efficiency or the impossibility of using such systems (for example, the aero-engines) determines the compressor section contamination [5].

The contamination is due to the adhesion of such micro-sized particles to the blade and vane surface, generating the gas turbine fouling phenomenon. This adherent layer determines the modification of the blade shape (especially the leading edge) and the modification of the surface roughness. These effects change the machine compressor performance over the operation time [7, 8]. To slow down these effects,

the engine was washed frequently [9, 10] during the operation, even if the performance restoration can be achieved by employing an offline washing procedure or machine overhaul [11 – 13].

The root cause of gas turbine fouling is not straightforward. The adhesion of the contaminant depends on blade/vane surface characteristics (the presence of coating and the surface roughness), the environmental condition (in particular, the relative humidity), and the operating point of the unit. Therefore, the adhesion results from several conditions and the effects on the unit performance. As reported in [14], for the same operating condition, two units could experience different adhesion patterns, and for the same adhesion pattern, two units could experience two different performance degradations (i.e., the machine susceptibility and sensitivity to fouling).

1.1. Aim of the work

A detailed investigation of the fouling phenomenon in terms of the adhesion process has to consider the location and intensity of the deposits. This work proposed a new methodology based on image analysis able to detect the deposits over the compressor flow path that could be adopted for lab-scale tests and during the overhaul operation. The proposed methodology is carried out on an actual engine after a controlled contamination process. The novelty of this approach is mainly due to its wide range of applicability. Pros, cons, and guidelines are also highlighted.

2. Materials and methods

A specific test bench has been set up to test the image detection of fouled compressor regions. The experimental rig was equipped with the compressor of the engine Allison 250 C18. This is a multistage axial unit coupled with a centrifugal stage able to reach an overall pressure ratio of 6.2 and a mass flow rate of 1.36 kg/s at the design speed of 51,600 rpm [15]. The centrifugal stage has two semivolutes, each with a circular exit duct with a diameter of 0.056 m. Two flexible tubes link the outlet ducts to an exhaust outlet with a diameter of 0.100 m. The compressor is driven by an electric motor. During the current test campaign, the compressor unit has been kept at 20,000 rpm, corresponding to 0.33 kg/s.

According to Fig. 1, the test bench is equipped with an external air treatment section, which allows the setup of the relative humidity at the compressor inlet, and a contaminant injection system, able to disperse micro-sized particles in the airflow swallowed by the unit. The particle feeder, the TOPAS SAG-410/U, can prepare and inject the solid contaminants with two Venturi eductors, guaranteeing the proper particle injection process. The contaminants were dosed using a variable-speed rotating ring to increase or decrease the mass per unit of time prepared for Venturi's sucking process. The dosing system and the setup of the contaminant injection are described in [16].

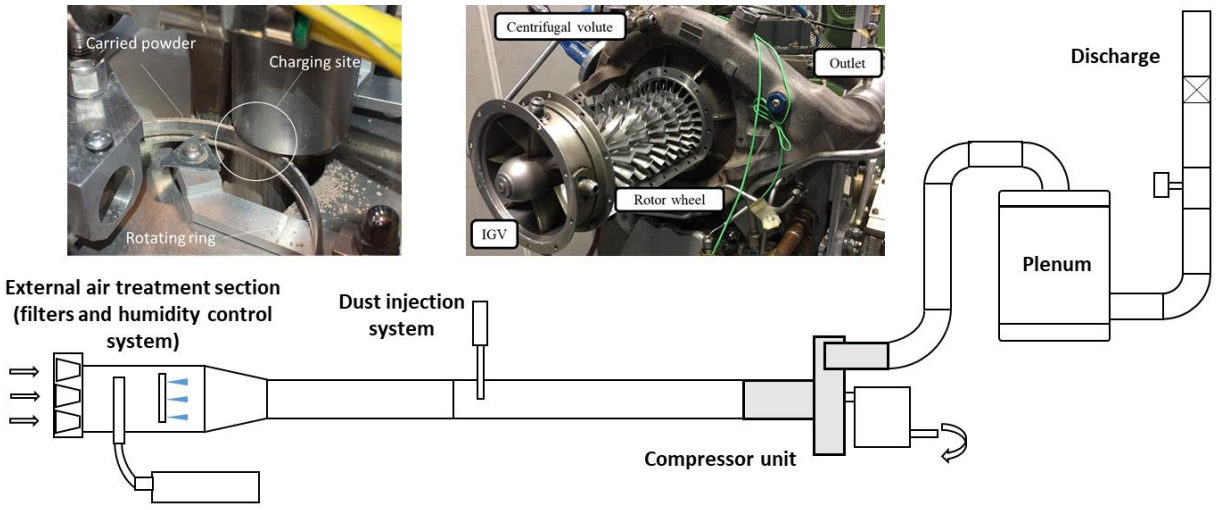

Figure 1. Test bench

2.1. Contaminants

To explore the fouling phenomenon, three powder samples have been considered. In line with the on-field experiences [3], soil particles come from several sources and have different diameters. In particular, the dust carried by the wind covers thousands of kilometers, and it is usually characterized by a diameter lower or almost equal to 1 μm. At the same time, bigger soil particles are typically carried by storms for a few kilometers [17, 18]. Therefore, three diameter distributions have been considered to explore the most comprehensive possibility. All of the soil samples are the Arizona Road Dust (ARD) sample, characterized by a density of 2717 kg/m^3. It is a natural-based powder consisting mainly of about 70 wt. % silica and 14 wt. % aluminum oxide and other minor iron, sodium, calcium, and magnesium oxides. To measure the diameters distribution, the Malvern Microsizer 3000 has been used. The particle diameter distributions for the three powder sample named ARD N (d_{mean} = 1.3 μm), ARD UF (d_{mean} = 4.8 μm), and ARD M (d_{mean} = 25.5 μm) are reported in Fig. 2. In Fig. 2, SEM (Scanning Electron Microscope) detections are reported. Looking at the detections, the soil particles are characterized by an irregular shape and edges. All of the powder samples are provided by Powder Tech Inc. (Powder Technology Inc., Arden Hills, USA).

2.2. Image and deposit detections

A set of images of the compressor flow path was taken during the experimental investigation to detect the deposits on the compressor blade and vane surfaces. A proper light and camera setup was adopted to ensure the repeatability of the detection process, allowing the comparison between the clean and fouled blades according to the different powder size distributions. The image detection was carried out by disassembling the compressor unit. Thanks to this, the half compressor case (stator) was positioned on a realized-on-purpose holder while the rotor was kept in the original position. Since the rotor was detected without any disassembling procedure, camera and light setups are installed directly on the rotating test rig (see Fig. 3). This fact implies several difficulties related to the proper detection of the flow path, mainly due to the thermal expansion of the compressor unit. Due to the lab-test conditions and the compressor geometry, the effects of the thermal expansion expire after five hours.

The deposit patterns are taken directly from the lab-testing facility employing dedicated cameras with a resolution of 3264 x 2448 pixels positioned to detect the entire flow path of the axial compressor divided according to the rotor and stator components. The white light setup is adopted for both parts of the compressor flow path with the intensity of 4000 K. In Fig. 3, the light setup for rotor and stator surfaces has been reported.

After the picture collection (clean and fouled conditions), the deposit patterns were determined through image processing based on the open-source package Image J [19] developed by the U.S. National Institutes of Health. The procedure [20 – 22] is based on subtracting the picture of the fouled surfaces and the picture of the clean one converting the resultant image into a binary format. Finally, the picture is converted to show the deposits as the grayscale-colored pattern on the picture. The procedure is summarized in Fig. 4.

2.3. Test matrix

To prove the capability of the measurement strategy to detect the fouled regions, a specific test matrix has been done. Since the adhesion process is strongly related to the combination of particle diameter

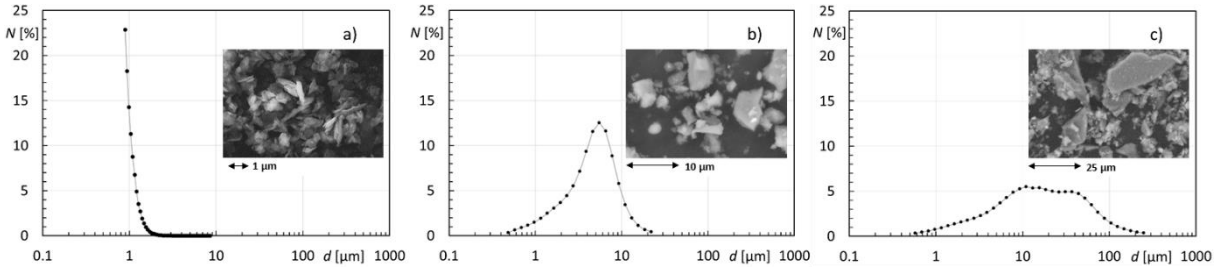

Figure 2. Particle diameter distributions: a) ARD N, b) ARD UF, and c) ARD M

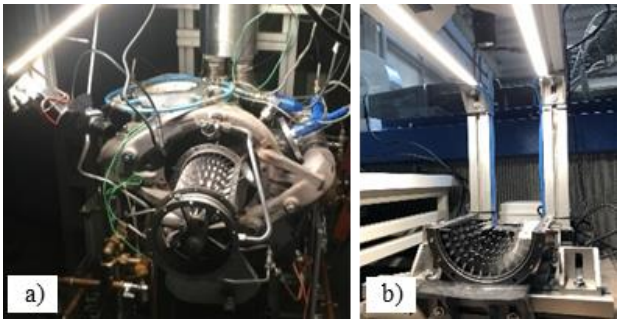

Figure 3. Light and camera setup for a) rotor and b) stator surfaces

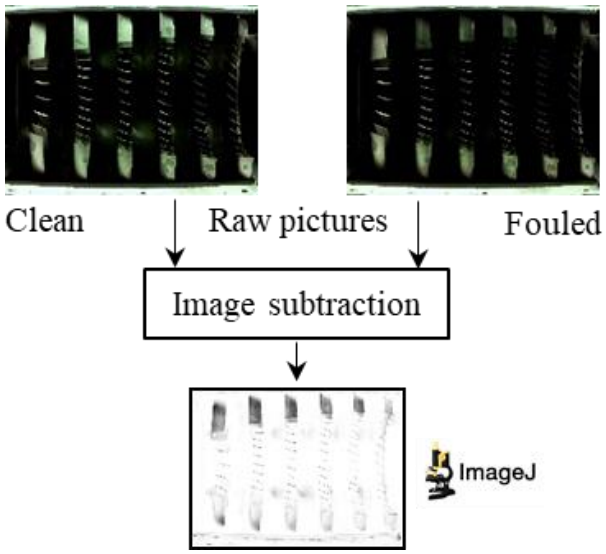

Figure 4. Strategy for the image post-process

and air humidity, the proposed analysis covers a humidity range of (15 – 80) %RH. Table 1 shows the tested conditions. The fouling tests cover the upper half-plane of the overall design. Each test had a duration of 4 hours. The powder concentration was kept constant and equal to 6 mg/m^3 for all the tested powders by adjusting the ring speed of the feeder (see Fig. 1 for more details).

To ensure the repeatability of the results, the compressor was thoroughly cleaned at the beginning of each test. First, the offline cleaning was done by disassembling the stator axial part to allow easy access to the rear stages of the compressor. Next, the stator and rotor blades, the shroud, and the hub were cleaned with demineralized water combined with a cleaner product and brushes to restore the initial condition of cleanliness. After the conclusion of the cleaning operation, pictures of the rotor and stator surfaces are taken. After the compressor start-up, the achievement of the desired operating point, and the assessment of the thermal equilibrium, the injection of the contaminant is carried out. The particle flow rate injected is kept constant for the test duration. At the end of each test, the axial part is disassembled, and fouled pictures are taken.

Table 1. Test matrix (× = tested; - = not tested)

	15 %RH	50 %RH	80 %RH
ARD N	×	-	×
ARD UF	-	×	×
ARD M	-	-	×

3. Results

The results of the present investigation are organized as follows. In the first part, an overview of detections is proposed to show the capability of this measurement process to detect different deposition patterns on compressor rotor and vanes surfaces. In the second part, a quantitative analysis has been proposed based on the image post-process. Finally, an assessment of the image analysis capabilities has been presented.

3.1. Image detections

Samples of image detections are proposed in Figs 5 – 7. These figures report the results from the deposition tests of ARD N with 15 %RH, ARD UF with 50 %RH, and ARD M with 80 %RH, respectively. The image reports the clean, fouled, and post-processed detections from left to the right. Concerning a single picture, the front stages are on the right, while the rear stages (axial compressor discharge section) are on the left.

Comparing the clean and fouled detections, it is possible to see the deposition process affecting the blade and vanes surfaces and the hub and shroud surfaces. Increasing the particle diameter, the adhesion process becomes less effective even with greater humidity. A greater deposition can be found in the pressure side of the rotor blade and stator vanes, as well as in correspondence with the leading edge. From Figs 5 – 7 is clear that using only the detection, a detailed comparison between the clean condition and the fouled one is not straightforward. In addition, by changing the contaminants, the comparisons became impossible. Based on the subtraction process between "fouled" and "clean" images, the image post-process allows the proper comparison. As seen from the analysis, the image-post process emphasizes the deposit patterns, generating a black-and-white map useful to consider how different contaminants and operating conditions affect the compressor surfaces. As reported in [23 – 26], the effects of deposits on compressor performance change according to the location on the blade surfaces. For example, the contamination on the suction side of the stator vanes changes over the stage, and only by using the post-processed images has it been possible to quantify. The smallest powder (ARD N) affects all stages, ARD UF affects only the first three stages, while the coarsest powder (ARD M) affects the first two stages with a thin and non-homogenous layer. Rotor detections are affected by the hub surface reflection due to a mirror-like surface finishing, determining the impossibility of defining the proper contamination of the rotor hub. In addition, the shadows due to the half-part of the stator that can not be dismounted increases the inaccuracy of the image detections.

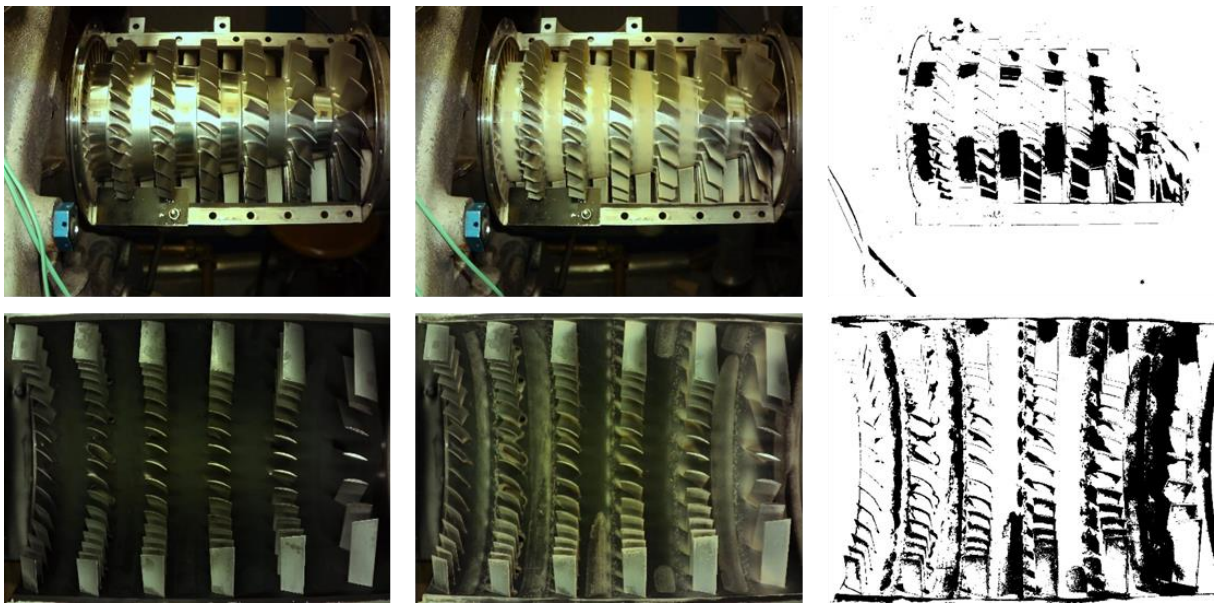

Figure 5. Detections (from left to right the clean, fouled, and post-processed images) for ARD N (15 %RH)

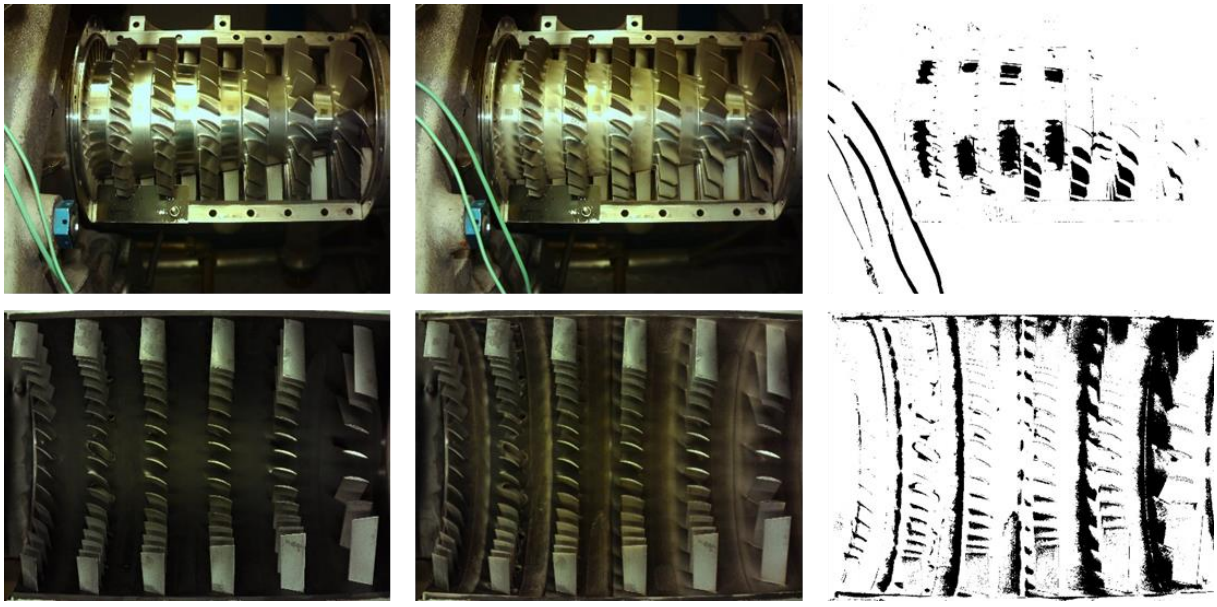

Figure 6. Detections (from left to right the clean, fouled, and post-processed images) for ARD UF (50 %RH)

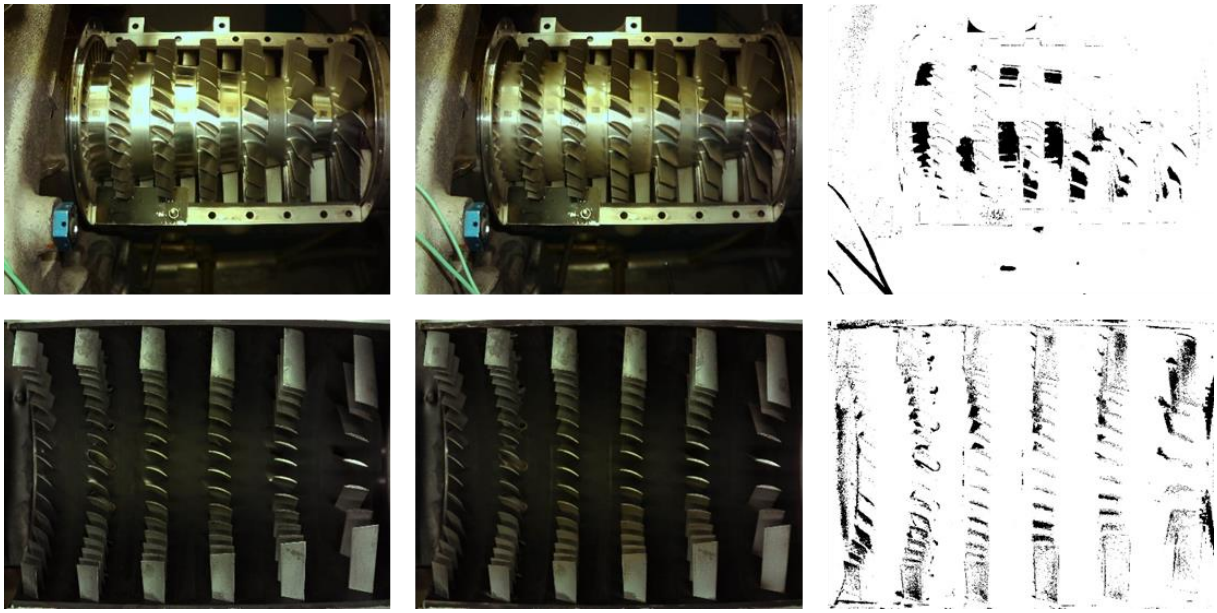

Figure 7. Detections (from left to right the clean, fouled, and post-processed images) for ARD M (80 %RH)

Regarding rotor surfaces, similar considerations can be made regarding contamination. The coarse powder (ARD M) does not determine relevant deposits concerning the smaller powder. In addition, the rotor surface is subjected to the centrifugal force that could be responsible for the detachment process of the deposits over the compressor operation [27].

The differences obtained by black and white images can be directly compared since the light intensity is the same for each test. This is due to the test bench setup and thanks to the powder color that does not change moving from the finest to the coarsest powder. The detections and the post-processed images reported in Figs 5 – 7 show that bigger particles are less prone to generate deposits on the compressor surfaces. The most affected regions are located at the suction side of the stator, in the proximity of the

hub driven by the separation phenomenon that characterizes this vane region. Similarly, the rotor suction side regions located at the blade tip are highly affected, especially in the case of ARD N. The pressure side shows contamination on the leading edge, clearly visible on the stator vane. Coarser powder samples (ARD UF and ARD M) generate a scattered pattern on the vane pressure side, probably due to their dimension, that can not generate a stable and compact layer on the surface [28, 29].

These results are in line with those reported in the literature [3] and show how the operating site of the unit can affect the degradation phenomenon due to fouling. Looking at the contamination over the compressor stages, the results demonstrate how the contamination decreases over the stages, in line with the data reported in [30]. These results depend on the compressor design and the operating points in terms of regime and inlet conditions [14]. In particular, with higher or lower humidity values, these patterns could be different from the first stages to the rear ones.

3.2. Quantitative analysis

Starting from the post-processed image, a quantitative analysis can be done. The black and white images allow the comparison of the dirty and clean areas on the compressor surface. Figure 8 reports the quantitative analysis of the ARD N test with low and high relative humidity values. The comparison is based on the pixel count of the post-processed images. According to the adopted calculation (see Fig. 4 for more details), black pixels represent the dirty regions, while white pixels represent the clean regions. Therefore, comparing the number of white and black pixels and the total pixel, it is possible to estimate the fouled portion of the interested surface. In Fig. 8, four representative pressure sides of the stator vane surfaces have been considered. The regions of interest for each vane have been highlighted with red lines. In these regions, the ImageJ software made a pixel count, and the ratio between white pixels and black pixels to the total number of pixels has been reported in pie charts. The increased humidity values determine more detrimental conditions increasing the adhesion capability of particles. At the same time, a quantitative explanation of the deposit modification over the compressor flow path can be done by looking at the pie charts. Greater humidity determines the greatest contamination of the first stage and a progressive reduction of the deposits. By contrast, for the same operating condition and contaminants but during a dry period, the compressor experiences more significant contamination on the rear stage instead of the first stage.

To increase the capability of the present post-process to give quantitative data, an evolution of this pixel comparison is reported in [31]. The black-and-white conversion generates a straightforward application of the pixel counting technique, but it leads to inaccuracies related to the choice of the

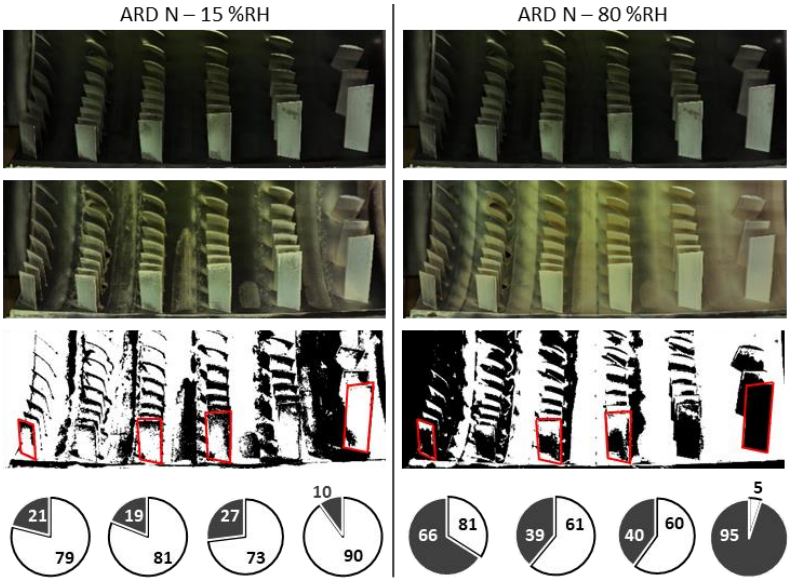

Figure 8. Sensitivity analysis to relative humidity for ARD N. The image analysis is dedicated to the pressure side of the stator vanes

threshold. In [31], a frequency analysis of the greyscale pixels has been done to prove the efficiency of compressor cleaners in removing soot particles from the blade surface.

3.3. Comparison

The final step of the present investigation is the assessment of the validity of the image analysis. Since image detection could be very effective in the on-filed application, using a lab-scale test, it is possible to define the reliability of the present procedure to represent a proper reference for future applications. To compare the image detection of the deposits (black and white pictures) with the actual intensity of the deposits, a procedure reported in [32, 33] has been carried out. The estimation of the deposited mass on the blade surface represents the basis for the proper comprehension of the fouling effects [34 – 36]. Therefore, the deposited dust on the compressor vanes has been measured employing an on-purpose designed device, the Localized Aspirator for Particle Observation (LAPO). The exploded view of the LAPO is depicted in Fig. 9. This device is a tool employed for particle sucking and measurement from surfaces driven by a vacuum pump. The system is based on a stainless steel needle with a diameter of 1 mm, which allows direct particle sucking from the surface of interest. In Fig. 9, the deposit collection from a stator vane leading edge is shown. The reported frames show the leading edge before and after the deposit collection, corresponding to the first passage time of the device. Depending on the stickiness of the deposited layer, a complete deposit removal can be achieved with multiple passages of the needle. The LAPO is equipped with a filter placement section allowing particle trapping and collection. At the end of the particle collection, the device is unscrewed, and the filter is removed and weighted to calculate the collected powder amount.

Figure 10 reports the mass of the deposits collected in correspondence to the pressure side of the stator vane surfaces. These quantitative measurements correspond to the same surfaces evaluated in Fig. 8. Comparing the analysis carried out by counting the pixel ratio and the collected mass, it can be concluded that the proposed measurement strategy allows an evaluation of the fouling phenomenon over the machine flow path. As can be seen from Fig. 10, front stages resulting from the high-humidity test are characterized by greater contaminant mass, similar to the results shown in Fig. 8. Image detection reveals the fouled area, and for this reason, comparing the deposited mass, some discrepancies could be detected. Looking at the aft stages, the deposited mass indicates that the relative humidity value does not affect the deposition process. By contrast, image detection shows greater contamination for the test with 80 % RH. In image detection, the deposited thickness is not detected, and a complete assessment of the deposited mass (i.e., volume) can not be assessed. The Shape From Shading (SFS) technique could represent a step forward in this sense. The SFS allows the obtainment of three-dimensional information starting from a two-dimensional detection. As shown in [37], this technique could be useful to estimate the deposit thickness even if, due to the mathematical constraints, the results have to be validated after a calibration procedure, reducing the applicability to on-field detection.

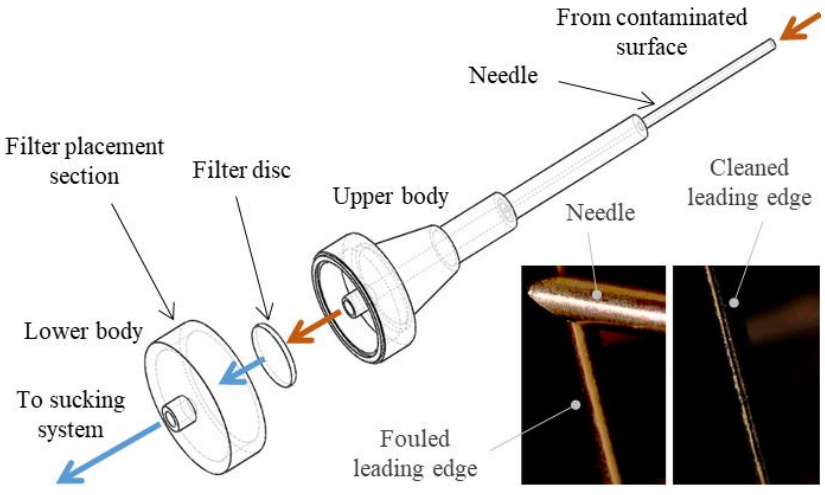

Figure 9. The LAPO system

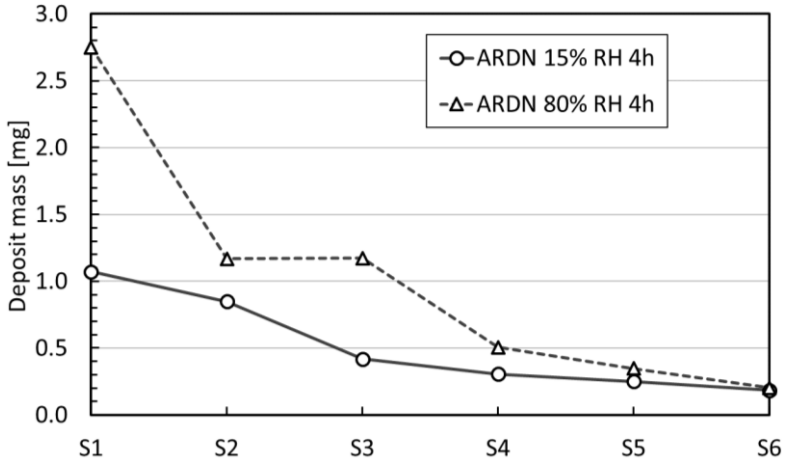

Figure 10. Mass deposits collected from the pressure side of the stator vanes

3.4. Remarks and guidelines

According to the results, it can be highlighted that image detection allows the recognition of the fouled region over the compressor flow path. The capability of the image analysis to detect the modification of the compressor surface is based on the proper light and camera setup and is easy to be assessed. Since image detection can be quickly done on-filed, during an inspection and/or overhaul, in this last section, some guidelines have been reported to make this technique affordable and applicable. The comparison between fouled (or damaged) sections and the clean (or restored) ones can be made by acquiring the proper set of images immediately before and after the restoration process. In this way, qualified operators can realize the image detection within the maintenance intervals and compare the surface deterioration with the data coming from the control system of the unit, putting the basis to increase the comprehension of the unit operation. To do this, some hints are reported in the following:

- install the cameras in a fixed position, excluding vibration and lens deterioration (dirty or powder due to operation on the construction site);
- use artificial light setup (make the photographic set overnight), paying attention to the light intensity (sometimes the light intensity changes due to voltage variation) and position (use the same light position before and after the restoring operations);
- detect several images from different perspectives. In this case, use multiple cameras to avoid the mount and dismount processes;
- use reference criteria (for example, a frame or fixed support) to have a fixed helpful point to compare the image and establish if the camera was moved or not;
- use a holding system to keep the compressor shaft in the same position before and after the overhaul process;
- cool down the unit, and remember that the thermal expansion could also be responsible for the deviation between clean and fouled conditions.

As shown in the previous paragraph, this technique is helpful in making a qualitative assessment of the contamination. A more precise detection to move this analysis from a qualitative to a quantitative framework should be based on the study of shading (SFS techniques) and the possibility of checking the image detection with options based on the quantitative assessment of the deposited layer [28, 29, 37].

4. Conclusions

In the present investigation, the capability of image detection to show a fouled 'pattern on an axial compressor unit has been proposed. Furthermore, a proper test bench has been developed to prove this fascinating measurement technique's capability. The test bench is based on an axial compressor, fouled with three different powders during the operation with three different relative humidity levels.

The analysis shows the capability of image detection to grasp the modification of the internal surface of the compressor as a function of the contamination process, leading to more detrimental conditions

with smaller powder and greater humidity levels. The contamination has been quantified using an open-source software tool, starting from a simple image comparison. Estimating the percentage area of each blade and vane surface covered by the contaminants has shown that image detection could represent valid support to detect the effects of fouling on compressor degradation. Finally, an estimation of the inaccuracy of the image detection method has been proposed showing that, in the case of non-uniform layer thickness, the analysis of the fouled area does not match with the estimation of the contaminant mass.

From the present results, it can be concluded that image detection and post-process could be helpful in detecting the effects of compressor operation in harsh environments and making a reference during the overhaul operation of land based-unit. Furthermore, if applied systematically, this method could feed a helpful database to correlate the machine operation with on-filed data and performance. A set of guidelines and key points were also listed to do this.

5. Acknowledgments

The authors wish to thank Eng. Luca Panetto for his valuable support in carrying out the tests and the data post-process.

6. References

[1] Dahl G and Suttrop F 1998 *Int. J. Hydrogen Energy* **23**, 695–704
[2] Palies P P 2022 Proc. ASME Turbo Expo, GT2022-78214, V001T01A002
[3] Kurz R and Brun K 2012 *J. Eng. Gas Turbines Power* **134**, 032401
[4] Diakunchak I S 1992 *J. Eng. Gas Turbines Power* **114**, 161-68
[5] Suman A, Morini M, Aldi N, Casari N, Pinelli and Spina P R 2017 *J. Turbomach.* **139**, 041005
[6] Suman A, Casari N, Fabbri E, di Mare L, Montomoli F and Pinelli M 2019 *Prog. Energy Combust. Sci.* **74**, 103-51
[7] Vulpio A, Suman A, Casari N, Pinelli M, Kurz R and Brun K 2021 *J. Eng. Gas Turbines Power* **143**, 081005
[8] Suman A, Vulpio A, Casari N and Pinelli M 2021 *Powder Tech.* **394**, 597-607
[9] Brun K, Grimley T A, Foiles W C and Kurz R 2015 *J. Eng. Gas Turbines Power* **137**, 042605
[10] Casari N, Pinelli, M, Spina P R, Suman A and Vulpio A 2021 *J. Eng. Gas Turbines Power* **143**, 031020
[11] Mund F C and Pilidis P 2004 Proc. ASME Turbo Expo **4**, GT2004-53224
[12] Asplund P 1997 Proc. ASME Turbo Asia Conference, 97-AA-135, V001T09A003
[13] Perullo C A, Lieuwen T, Barron J, Grace D and Angello L 2015 Proc. ASME Turbo Expo **3**, GT2015-43736
[14] Meher-Homji C B, Chaker M and Bromley A F 2009 Proc. ASME Turbo Expo **4**, GT2009-59239, 571-90
[15] Munari E, Morini M, Pinelli M, Spina P R and Suman A 2017 *J. Eng. Gas Turbines Power* **139**, 022605
[16] Suman A, Vulpio A, Fortini A, Fabbri E, Casari N, Merlin M and Pinelli M 2021 *Int. J. Heat Mass Transfer* **165**, 120632
[17] Gómez-Moreno F J, Pujadas M, Plaza J, Rodríguez-Maroto J J, Martínez-Lozano P and Artíñano B 2011 *Atmos. Environ.* **45**, 3169-80
[18] Wang G H, Zhou B H, Cheng C L, Cao J J, Li J J, Meng J J, Tao J, Zhang R J and Fu P Q 2013 *Atmos. Chem. Phys.* **13**, 819-35
[19] Schneider C A, Rasband W S and Eliceiri K W 2012 *Nat. Methods* **9**, 671-75
[20] Suman A, Vulpio A, Casari N, Pinelli M, Kurz R and Brun K 2021 *J. Eng. Gas Turbines Power* **143**, 081006
[21] Casari N, Pinelli M, Suman A, Vulpio A, Appleby C and Kyte S 2020 *J. Glob. Power Propuls. Soc.* **4**, 253–63
[22] Casari N, Pinelli M, Suman A and Vulpio A 2022 *CEAS Aeronaut. J.* **13**, 113-25
[23] Morini M, Pinelli M, Spina P R and Venturini M 2010 *J. Eng. Gas Turbines Power* **132**, 072401
[24] Morini M, Pinelli M, Spina P R and Venturini M 2011 *J. Eng. Gas Turbines Power* **133**, 072402

[25] Aldi N, Morini M, Pinelli M, Spina P R, Suman A and Venturini M 2013 *J. Turbomach.* **136**, 021016
[26] Aldi N, Morini M, Pinelli M, Spina P R, Suman A, Venturini M 2013 *Energy Procedia* **45**, 1057-66
[27] Friso R, Suman A, Vulpio A, Zanini N, Casari N, Pinelli, M 2023 *Int. J. Heat Mass Transfer* **200**, 123525
[28] Suman A, Vulpio A, Casari N, Pinelli M, di Lillo F and D'Amico L 2022 *Powder Tech.* **394**, 608-21
[29] Suman A, Vulpio A, Pinelli M and D'Amico L 2022 *J. Eng. Gas Turbines Power* **144**,101010
[30] Tarabrin A P, Schurovsky V A, Bodrov A I, and Stalder J-P 1998 Proc. ASME Turbo Expo **4**, 98-GT-416, V004T11A006
[31] Vulpio A, Suman A, Casari N, Pinelli M, Appleby C and Kyte S 2021 Proc. ASME Turbo Expo **8**, GT2021-59455, V008T20A013
[32] Vulpio A, Suman A, Casari N and Pinelli M 2022 *J. Turbomach.* **144**, 71009
[33] Vulpio A, Suman A, Casari N and Pinelli M 2021 *Aerospace* **8**, 81
[34] Suman A, Kurz R, Aldi N, Morini M, Brun K, Pinelli M and Spina P R 2014 *J. Turbomach.* **137**, 021009
[35] Suman A, Morini M, Kurz R, Aldi N, Brun K, Pinelli M and Spina P R 2015 *J. Turbomach.* **137**, 021010
[36] Suman A, Kurz R, Aldi N, Morini M, Brun K, Pinelli M and Spina P R 2016 *J. Eng. Gas Turbines Power* **138**, 012603
[37] Casari N, Fortini A, Pinelli M, Suman A, Vulpio A and Zanini N 2022 *Measurement* **187**, 110185